Available online at www.sciencedirect.com
ScienceDirect
Catalysis Today 129 (2007) 86–95
CATALYSIS TODAY
www.elsevier.com/locate/cattod

Photocatalytic behavior of suspended and supported semiconductor particles in aqueous media: Fundamental aspects using catechol as model molecule

Teresa Lana-Villarreal *, Damián Monllor-Satoca, Antonio Rodes, Roberto Gómez *

Departament de Química Física i Institut Universitari d'Electroquímica, Universitat d'Alacant, Apartat 99, E-03080 Alacant, Spain

Available online 6 August 2007

Abstract

The interaction and photoreactivity of catechol with both anatase and WO_3 nanoparticulate samples have been investigated by applying different experimental techniques. Infrared and Raman spectroscopies have been combined to study catechol adsorption from acidic aqueous solutions. Adsorbed (chelating) catecholate is detected on both oxides together with molecularly adsorbed catechol in the case of anatase. The adsorptive behavior in the dark is completed with a parallel study with a quartz crystal microbalance, showing that upon catechol adsorption the hydrophilic–hydrophobic properties of the oxide nanoporous film vary. Adsorbed catecholate behaves as a charge transfer complex, which can be excited with visible light, as evidenced by Raman Spectroscopy, making possible photocatalytic activity under visible illumination. The time evolution of the Raman spectra shows an increasing fluorescence indicating that, upon electron injection, polymerization of catechol takes place at the semiconductor surface. The polymerization rate is found to be orders of magnitude larger for sintered nanoparticulate thin films than for slurries. Laterally resolved photoelectrochemical experiments evidence that electrons photoinjected by the adsorbed catecholate are highly delocalized through the nanoporous matrix. The advantages of employing a multi-technique approach for investigating adsorptive and photocatalytic events from a physicochemical point of view are outlined. Particular attention is paid to both hydrophobic and electron delocalization effects as they contribute to confer to the nanoparticulate sintered films specific properties not found in suspensions to the same extent.

Keywords: Photocatalytic behavior; Semiconductor; Aqueous media; Catechol

1. Introduction

Heterogeneous photocatalysis is one of the most promising oxidation technologies for wastewater treatment. An increasing attention has been devoted to this issue since the appearance of the first related publication in 1976 [1]. Nowadays several reviews are available regarding both fundamental and technological aspects [2–8]. Most of them focus on TiO_2 as photocatalyst, being used either suspended in solution or supported on a solid substrate. Often the immobilization of TiO_2 particles reduces their photocatalytic efficiency due to a diminution of active surface area [9] and to mass transport limitations [9,10]. However, this strategy shows several advantages from a practical viewpoint. First, photocatalysts can be used in continuous processes avoiding the filtration step for removal of the semiconductor particles after water purification. Secondly, it is feasible to work with configurations in which all the catalyst particles are illuminated [11].

Heterogeneous photocatalytic reactions are complex processes far from being fully understood. Not only oxidation and reduction reactions take place in the same particle surface (in the absence of an applied potential) but adsorption/desorption of reactants, intermediates and/or products may lead to different oxidation pathways. Therefore, it is advisable to independently study the different factors that determine the global process efficiency. Within this context, we believe that a multifaceted physicochemical investigation of model systems in heterogeneous photocatalysis is a valid approach that can contribute to improve both our understanding of the

* Corresponding author. Fax: +34 965903537.
E-mail addresses: Teresa.Lana@ua.es (T. Lana-Villarreal), Roberto.Gomez@ua.es (R. Gómez).

0920-5861/$ – see front matter © 2007 Elsevier B.V. All rights reserved.
doi:10.1016/j.cattod.2007.06.050

photocatalytic events and our ability to design in a rational way new photocatalysts. The oxidation and reduction processes can be separately studied by electrochemical methods [12], while the adsorption (and reactivity under illumination) can be measured by different methods such as the quartz crystal microbalance (QCM) [13] or by monitoring changes in the solution concentration [9–10,13]. In addition, it is highly desirable to complete these macroscopic measurements, which lack of chemical specificity, with microscopic approaches to the semiconductor-solution interface. In this sense, in situ vibrational spectroscopy techniques, such as infrared and Raman spectroscopies, provide valuable and unique information on the interface under both reactive and non-reactive conditions. Infrared spectroscopy is a mature technique well-known by its high sensitivity and broad applicability [14]. On the other hand, laser Raman scattering techniques present some advantages, being particularly important the low scattering cross section of water molecules, which allows the acquisition of single beam absolute spectra. Although its sensibility is low, it can be enhanced by resonance and surface enhanced scattering mechanisms [15].

Along these lines, we have chosen catechol as a model molecule for heterogeneous photocatalysis studies motivated by several reasons. First, it has been considered in the literature as a model contaminant by itself [16]. It is also an intermediate in the well-studied photocatalytic degradation of phenol [17]. Moreover it is known to form upon adsorption on oxide surfaces, surface charge-transfer complexes (SCTC) excitable with visible light [18], which makes possible its study by visible-laser resonance Raman spectroscopy (RRS). It is worth noting that although we have used the expression ''heterogeneous photocatalysis'' for the SCTC reaction (photosensitized reaction), the mechanism of the corresponding photooxidation under visible illumination differs from that of typical heterogeneously photocatalyzed reactions. In the latter, what gets excited is the photocatalyst itself rather than a SCTC.

The article is organized as follows. Initially, the adsorption of catechol in the dark is studied on porous TiO_2 and WO_3 thin films by attenuated total reflection infrared (ATR-IR) and RRS, identifying the adsorbates present on both oxides. A parallel study with a QCM reveals changes in the hydrophobic/hydrophilic properties of the semiconductor films during the adsorption process. Finally, the system is studied under reactive conditions (visible illumination) by Raman spectroscopy and by a laterally resolved photoelectrochemical method. The practical implications of these results are discussed in detail, paying particular attention to the reasons underlying the different photocatalytic behavior of suspensions and sintered nanoparticulate thin films.

2. Experimental

2.1. Chemicals and materials

Commercial titanium dioxide (anatase, Alfa-Aesar, APS 32 nm) and monoclinic tungsten trioxide (PI-KEM, APS 50 nm) nanopowders were used. All solutions were prepared using catechol (Aldrich, +99%), $HClO_4$ (Merck, p.a. 60%) and Millipore Elix3 water.

2.2. Infrared spectroscopy

The ATR-IR measurements were carried out with a Nicolet Magna 850 spectrometer equipped with a MCT detector and a variable angle Veemax specular accessory (Pike Technologies). All the experiments were done in a cell provided with a semicylindrical ZnSe prism onto which the semiconductor films were coated by applying a small volume of oxide aqueous suspension and drying overnight in air at 50–60 °C. The ATR-IR spectra for adsorbed catechol on TiO_2 and WO_3 are presented as $-\log(R/R_0)$, where R_0 corresponds to the single beam spectrum obtained for each semiconductor film in a catechol-free solution.

2.3. Raman spectroscopy

Raman spectra were recorded with a confocal LabRam spectrometer from Jobin-Yvon Horiba with a Peltier cooled charge-couple detector. The excitation line was provided by a 50 mW Ar^+ laser (514.5 nm), focused through a 50*x* objective on the sample surface. RRS was performed on WO_3 and TiO_2 slurries and thin films. Slurries with a concentration of 0.16 g ml^{-1} in 0.1 M $HClO_4$ and 14.5 mM catechol were placed in an 80-μm thin layer cell equipped with a fused silica window. The thin films were prepared on F-doped SnO_2 (FTO, Asahi Glass Co, Japan) by electrophoresis [19] or by *doctor blading* a WO_3 concentrated suspension [20]. The films were allowed to dry before thermal treatment at 450 °C in air.

2.4. Quartz crystal microbalance

A quartz crystal microbalance model QCM100 from Stanford Research System (SRS) was used with commercial chrome/gold-coated 5 MHz quartz crystals (SRS). A suspension (0.6 g ml^{-1}) of anatase containing acetylacetone and TritonX-100 was spread over the quartz crystals. The samples were dried at ambient temperature before sintering at 350 °C for 30 min in air. The resonant frequency was measured in the presence of 0.1 M $HClO_4$, while the concentration of catechol was modified by successive additions of small volumes of a concentrated solution in 0.1 M $HClO_4$. The plotted resonant frequency shifts correspond to stationary conditions. In fact, the values were taken once the frequency stabilized, which took at least 8 min after each solution addition.

2.5. Laterally resolved photopotential measurements

A detailed description of the experimental setup can be found elsewhere [21]. Briefly, a mechanically modulated laser is focalized on the semiconductor thin film by means of an inverted optical microscope, which is equipped with a computer-controlled motorized *x*–*y* stage. As the platform moves, the illuminated spot at the semiconductor film is displaced, making possible to relate the measured

photopotential with the spot position. In these experiments, the anatase thin films were prepared on FTO substrates with two electrically isolated areas by spreading an anatase concentrated suspension as in the QCM experiments. A 514.5 nm Ar^+ laser (Melles Griot) was focused on the surface sample, defining a 40 μm diameter spot. The counter and reference electrodes were a platinum wire and a Ag/AgCl/KCl (3.5 M) electrode, respectively.

3. Results and discussion

3.1. Adsorption studies by means of vibrational spectroscopies

In this section we present results on the adsorption of catechol from acidic aqueous solutions on both TiO_2 and WO_3. In addition to the identification of the reactant adsorption geometry by a combination of Raman and IR spectroscopies, we illustrate the use of the latter to study the adsorption kinetics. In principle, both types of studies are relevant steps toward understanding and eventually improving the behavior of photocatalysts. On the other hand, as far as we know and apart from a very recent report by us [20], this is the first in situ vibrational adsorption study at the WO_3/solution interface.

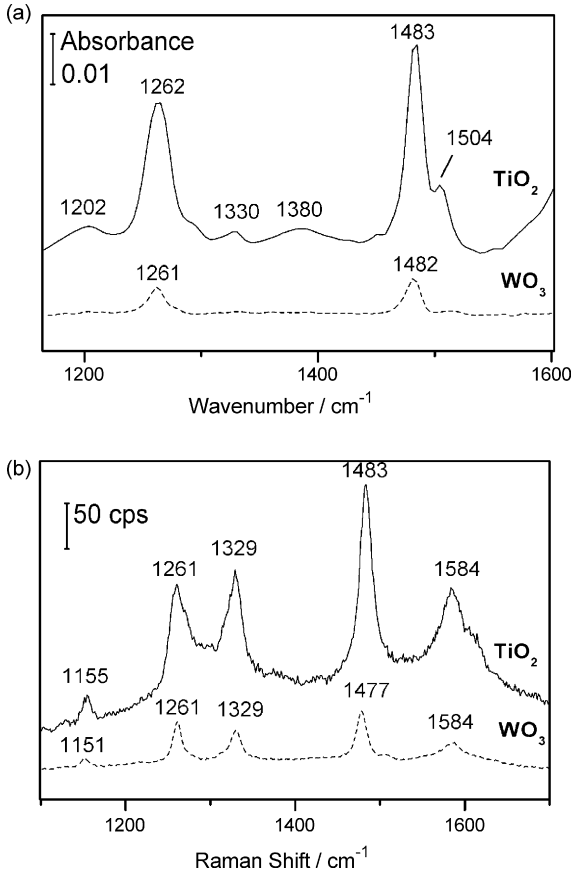

Fig. 1. (a) ATR-IR spectra for catechol adsorbed on TiO_2 and WO_3 in contact with 0.1 M $HClO_4$ solutions containing 25 mM and 20 mM of catechol, respectively and (b) Raman spectra obtained for TiO_2 and WO_3 slurries in contact with 0.1 M $HClO_4$ and 14.5 mM catechol solutions. The excitation line was provided by an Ar^+ laser at 514.5 nm.

Fig. 1(a) shows the ATR-IR spectra obtained for TiO_2 and WO_3 nanoporous thin films in contact with a 0.1 M $HClO_4$ + 20 mM catechol solution. Both spectra show intense bands at 1262 and 1483 cm^{-1} together with a weaker feature at 1330 cm^{-1}. Very similar spectra have recently been observed for catechol adsorption on Degussa P-25 at pH 6.2 [22]. Furthermore, in the case of anatase, additional bands can be distinguished (see below). All the bands correspond to adsorbates because, at this concentration and in the absence of the semiconductor thin films, no comparable bands coming from the solution species could be detected. The intensity of the bands is significantly higher in the case of the anatase film, indicating that the number of active adsorption sites being probed is also larger for this sample. Note that WO_3 and TiO_2 thin films are composed of particles of different size (see Section 2).

The stoichiometry and configuration of the adsorbate species can be determined by contrasting the recorded spectra with those of catechol aqueous solutions at different pH values and those of dissolved catechol complexes, such as $[Ti(cat)_2]_2^{2-}$ or $[Ti(cat)_3]^{2-}$ [19]. A comparison between the spectra of the adsorbate and catechol dissolved in alkaline solutions indicates that catecholate is the main adsorbed species on both semiconductors. In addition, the similarity of spectra in Fig. 1a with those for $[Ti(cat)_2]_2^{2-}$ and $[Ti(cat)_3]^{2-}$ complexes indicates that the adsorbate adopts a chelating configuration on both oxides, forming a five-atom ring in which both oxygen atoms of catecholate bind a Ti(IV) or W(VI) adsorption site. The alternative bridging structure, where the adsorbed catecholate binds two neighboring metallic sites does not seem to be energetically favored [23], at least in the case of TiO_2. Importantly, several W(VI) complexes with chelating catechol ligands have also been described [24,25].

The adsorption geometry in this particular case provides key information for the design of photocatalysts. In fact, the formation of adsorbed chelating species on both oxides can only be explained if each Ti(IV) or W(VI) surface atom has two available dangling bonds, which will occur at coordinatively unsaturated sites (CUS). Hence, photocatalysts with significant amounts of CUS would be desirable for catechol adsorption. As these sites are located frequently at kinks and steps, small quasi-spherical nanoparticles would be particularly indicated as photocatalysts, not only because they have a higher specific surface area but also because the fraction of CUS is maximized. It should be kept in mind, however, that the overall photocatalyst efficiency could be low, as these defects could also play the role of recombination centers. In addition, such small nanoparticles could be unstable in the long term.

As mentioned above, in the spectrum of catechol adsorbed on anatase, additional bands appear at 1202, 1380 and 1504 cm^{-1}, which are absent in dilute (<1 mM) catechol solutions as previously reported [19,22,26]. The bands at 1202 and 1380 cm^{-1} correspond to δ_{OH} modes, while the band at 1504 cm^{-1} has been attributed to a combination of $\nu_{CC} + \delta_{CH}$, typical of undissociated catechol [19]. Importantly, these bands are significantly different from those of a catechol solution in 0.1 M $HClO_4$ [19], thus excluding that they are simply due to solution species. Therefore, we can conclude that, on TiO_2, two

adsorbates are present: a chelate species and molecularly adsorbed catechol (at high enough solution concentrations). The existence of physisorbed species for concentrated solutions (>0.05 M) was also evidenced, on the basis of ATR-IR measurements, in the case of the 4-chlorocatechol/anatase system [27]. Significantly, under the same experimental conditions (Fig. 1a), only the chelating species was detected in the case of WO_3. In principle, the highly acidic character of WO_3 can explain this behavior. Contrarily to TiO_2, WO_3 surface is electrically neutral or even negatively charged in contact with 0.1 M $HClO_4$ solutions [28], which would not favor the adsorption of Lewis bases. Only if the adsorbate could interact strong enough with the acidic surface sites, adsorption would take place, as probably occurs in the chelating configuration. More importantly, as W(VI) is a strong Lewis acid, it should interact strongly with terminal OH groups. Catechol molecules may not be able to displace them from the surface, precluding the formation of a van der Waals bond between an oxygen atom of catechol and the W(VI) surface site [19,23].

It is worth noting that the aqueous suspensions of both oxides slightly darken in the presence of dissolved catechol, i.e. upon catechol adsorption both semiconductor samples absorb visible light [18,29]. In such a case, we can take advantage of the Raman spectroscopy to confirm the nature of the adsorbate and, more importantly, to identify the adspecies that is responsible for the photocatalytic activity in the visible (SCTC), as it will be the only probed by RRS. This is particularly useful in the case of anatase, where two adsorbates were identified by ATR-IR.

The Raman spectra for catechol adsorbed on TiO_2 and WO_3 are nearly identical (see Fig. 1(b)). They are dominated by four bands, which can be assigned to the ring stretching (1483 cm^{-1}) and ν_{CO} (1261, 1329, 1584 cm^{-1}) vibration modes. A less intense band at 1155 cm^{-1} can be ascribed to an in-plane CH bending mode. From the similarities with the spectra for alkaline catechol solutions and for the $[Ti(cat)_3]^{2-}$ complex, as well as from the absence of OH vibration modes, it can be concluded that the species monitored by RRS is the chelating catecholate dianion [19]. Therefore, this is the species originating the SCTC on both oxides. The spectral features related to catechol molecularly adsorbed on TiO_2 do not appear, meaning that it does not absorb the 514.5-nm laser light and it is thus not responsible for the photoactivity in the visible.

On the other hand, to assess the performance of a certain photocatalyst according to its adsorptive behavior, it is not only important to evaluate its equilibrium adsorption properties but also its kinetic adsorptive properties. In this respect, it has recently been proposed that kinetic limitations in the adsorption process could be at the origin of the dependence of the Langmuir–Hinshelwood model constants on light intensity [30,31]. Time-resolved ATR-IR experiments constitute a powerful tool for analyzing the adsorption kinetics on oxide nanoparticulate layers, although it has only been employed on a few occasions [32].

Fig. 2 shows the temporal evolution of the integrated intensity of the IR band at 1262 cm^{-1} for nanoporous films of TiO_2 (Abs_{TiO2}) and WO_3 (Abs_{WO3}). At low coverage, i.e. at small time values, the adsorption is very rapid, but as the coverage increases the number of available sites diminishes, and the rate decreases until the equilibrium is attained.

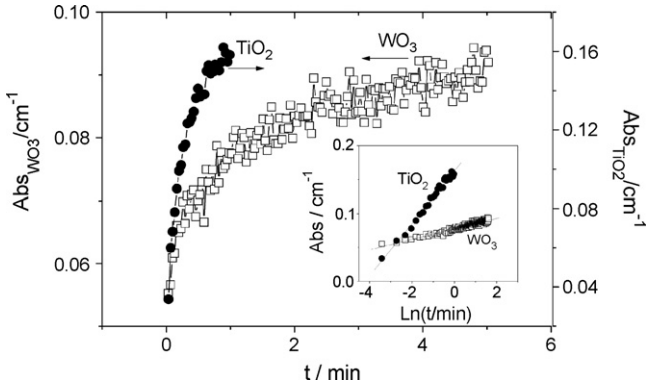

Fig. 2. Adsorption kinetics for catechol in 0.1 M $HClO_4$ on TiO_2 and WO_3 nanostructured films. At time 0 min a concentrated solution was added increasing the solution concentration up to 13 mM.

One of the most used models for studies of chemisorption reactions, especially at the solid/solution interface, is based on the Elovich equation:

$$\frac{dq}{dt} = a\exp(-\alpha q) \tag{1}$$

where q is the amount of solute adsorbed at time t, and α and a are constants. This equation has been applied to studies on the adsorption of several gases [33], metal ions [34] and anions [35] on porous systems. The constant a can be regarded as the initial adsorption rate since $\frac{dq}{dt} \to a$ when $q \to 0$. On the other hand, as initially (for $t = 0$) no catechol molecules are adsorbed ($q = 0$), Eq. (1) can be integrated, yielding:

$$q = \left(\frac{1}{\alpha}\right)\ln(t + t_0) - \left(\frac{1}{\alpha}\right)\ln t_0 \tag{2}$$

where $t_0 = 1/\alpha\ a$. If $t \gg t_0$ Eq. (2) can be simplified to:

$$q = \left(\frac{1}{\alpha}\right)\ln(t) + \left(\frac{1}{\alpha}\right)\ln \alpha a \tag{3}$$

The inset in Fig. 2 shows plots for Abs_{TiO2} versus ln (t) and Abs_{WO3} versus ln (t). Acceptable linear relations are obtained in both cases. Fitting the experimental data to Eq. (2) the values of α and a for both oxides were obtained. Interestingly, a, the initial adsorption rate is 156 $cm^{-1}\ min^{-1}$ for WO_3 while for TiO_2 the value decreases to 2 $cm^{-1}\ min^{-1}$. α is also larger for WO_3 (128 cm) than for TiO_2 (23 cm), meaning that, as the catechol coverage increases, the adsorption rate drops much faster for WO_3 than for TiO_2. Note that from the values of α and a, t_0 varies from 5×10^{-5} min for WO_3 to 2×10^{-2} min for TiO_2. Hence, the assumption $t \gg t_0$ made in Eq. (3) is justified in the time scale of our measurements. Although α has been related to the number of sites available for adsorption [34], the experimental data contradicts this hypothesis. The ATR-IR band intensity is smaller for WO_3, which can be associated to a smaller number of adsorbed molecules, i.e. a smaller number of adsorption sites available under our working conditions.

Importantly, such a constant has also been related to the adsorption energy distribution, which seems compatible with our results [36]. Nonetheless, it is important to note that mathematical expressions akin to Eq. (1) can be obtained by assuming different adsorption rate-controlling processes, including bulk and surface diffusion.

In any case, the rate of adsorption in the inner part of the film (in the ATR-IR experiment using a ZnSe prism only a few hundreds of nanometers in the inner part of the film are probed) can be estimated, thus providing information useful to design supported photocatalyst reactors. For instance, the thickness of the film is expected to affect the kinetics/extent of adsorption as the distance to be traveled by the organic species through the nanoporous channels increases.

In the same way, guidelines for the rational design of composite photocatalysts can also be derived from this type of experiments. For instance, results presented above, show that the initial adsorption rate of catechol on WO_3 is faster than on anatase. Therefore, mixing anatase and WO_3 in a composite photocatalyst would be beneficial because of the creation of bifunctional sites at the junctions between both materials that could share the higher reactivity of anatase and the faster adsorption kinetics on WO_3. This effect would add up to the charge separation enhancement at the junctions caused by band edge energy offsets. We may then substantiate, even quantitatively, the rationale given for explaining the increase in the photocatalytic activity observed upon coupling titania with WO_3 [37].

As mentioned before, one of our goals in writing this article is to emphasize the main differences that could appear between immobilized and suspended photocatalyst particles. In addition to the frequently invoked mass transfer limitations, diminution in the surface active area or higher tendency to poisoning, we will give evidence for further physicochemical effects that should also be taken into account. Quartz crystal microbalance and fluorescence measurements will serve to this aim.

3.2. Quartz crystal microbalance measurements

In principle, the quartz crystal microbalance is also a very sensitive tool to study surface reaction processes. QCM provides a simple way to measure changes in mass as the quartz crystal resonant frequency can be associated to them by means of the Sauerbrey equation:

$$\Delta f = -\frac{2 f_0^2}{A\sqrt{\rho_q \mu_q}} \Delta m \tag{4}$$

where Δf is the resonant frequency change, f_0 is the fundamental frequency of the QCM device, A is the electrode area, ρ_q is the quartz density, μ_q is the shear modulus of quartz and Δm is the mass change. However, only in few publications this technique has been employed to study adsorption and photocatalytic reactions on nanoporous TiO_2 layers [13,38–40]. Such a scarcity of papers is probably motivated by the difficulties, both experimental and interpretative, inherent to its use with nanoporous layers in contact with aqueous solutions [41].

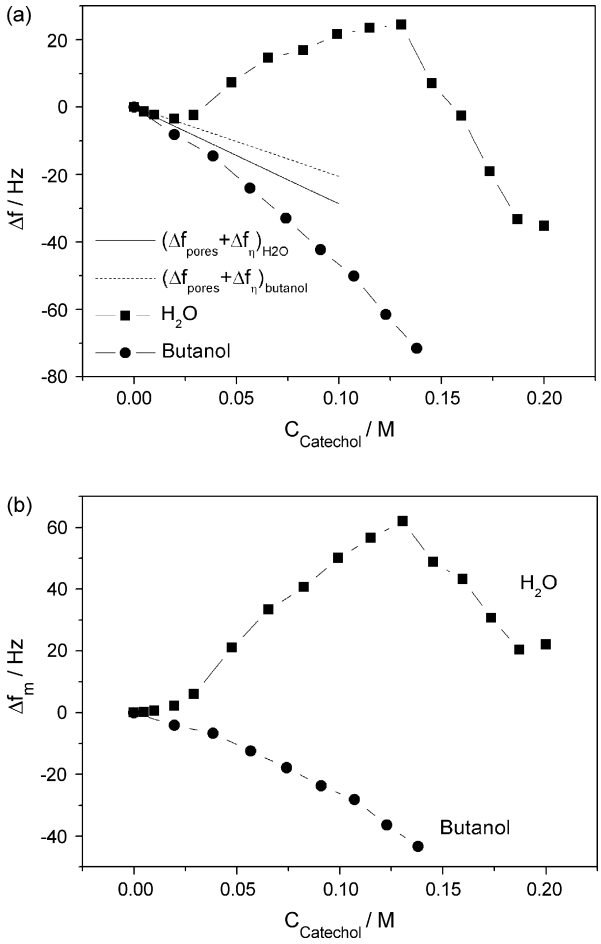

Fig. 3. (a) QCM frequency shift as a function of catechol concentration in aqueous solution (■) and in isobutanol (●), in the presence of 0.1 M $HClO_4$ together with estimated ($\Delta f_\eta + \Delta f_{pore}$) and (b) QCM corrected frequency shift (Δf_m) as a function of catechol concentration.

Fig. 3a shows the resonant frequency shift for a quartz crystal coated with TiO_2 particles upon the stepwise addition of different concentrations of catechol (■) in aqueous 0.1M $HClO_4$. Interestingly, at low concentrations the resonant frequency shifts to larger values with increasing catechol concentration while at high concentrations the opposite is observed.

For our particular system (nanoporous layer in contact with a liquid solution), the measured shift in frequency associated to the increase in catechol concentration should correspond to:

$$\Delta f = \Delta f_m + \Delta f_\eta + \Delta f_{pore} \tag{5}$$

where Δf_m reflects the change in mass due to the adsorption on the TiO_2 matrix, Δf_η represents the viscosity effect (in the outer film surface) [42] and Δf_{pore} is the frequency shift associated to the change in mass of the liquid in the pores [43]. Both Δf_η and Δf_{pore} can be estimated a priori. In a first approximation, the latter contribution will be proportional to the change in solution density and can be expressed as:

$$\Delta f_{pore} = \frac{-KV_{pore}\Delta\varphi_{sol}}{A} \tag{6}$$

where K is the QCM constant (in Hz cm^2 μg^{-1}), A is the probe geometric surface area, V_{pore} is the volume of the pores in the oxide film and $\Delta\varphi_{sol}$ is the change in solution density. Eq. (6) is valid as long as the solution in the pores has the same composition than in the bulk. In our particular case, we will assume a porosity of 50%, and we will take into account the solution density values [44].

On the other hand, Δf_η can be calculated, as proposed by Kanazawa et al. [42], according to:

$$\Delta f_\eta = -K\sqrt{\frac{\Delta\eta\Delta\varphi_{sol}}{\pi f_0}} \quad (7)$$

where $\Delta\eta$ is the change in viscosity caused by the introduction of catechol. It can be estimated from literature viscosity data [44].

In Fig. 3a, the calculated values for $(\Delta f_\eta + \Delta f_{pore})$ in water have been included. As observed, both contributions are negative. In Fig. 3b, Δf_m, calculated as $\Delta f - (\Delta f_\eta + \Delta f_{pore})$, is plotted against the added catechol concentration. One could think that Δf_m should also be negative, as an increase in mass should accompany catechol adsorption. Interestingly, the observed behavior is at odds with this expectation and three regions can be distinguished. For catechol concentrations lower than 0.02 M, Δf_m is rather small although adsorption is known to have occurred from the spectroscopic experiments and also from the darkening of the oxide films associated to the formation of the SCTC. The behavior is even more striking in the intermediate catechol concentration range (0.02–0.13 M) as successive additions of the organic substrate lead to increases in the frequency that cannot be explained in a straightforward way. For high enough concentrations (above 0.13 M), further additions of catechol lead to the expected decrease in frequency.

Two main factors with important implications in heterogeneous photocatalysis reactions can account for the unexpected behavior at low and intermediate concentrations: (a) the adsorbate may replace a certain number of solvent molecules from the interface, (b) the repulsion of water, mainly inside the pores, but also at the outer surface of the TiO_2 film. The latter effect would be induced by the hydrophobic character imparted by catechol adsorbed molecules to the inner and outer TiO_2 surface. As shown above, the adsorption of catechol leaves the highly hydrophobic aromatic ring directed towards the solution phase, which would explain the observed hydrophobic effect. Several authors have previously demonstrated that despite adsorption occurring on the film surface, apparent decreases in mass, associated with the adsorbent-imparted hydrophobicity can be measured for porous but also for non-porous substrates [40,45,46].

The behavior in the low concentration region would be dominated by the substitution of interfacial water by adsorbed catechol. The region of intermediate coverage is characterized by a significant frequency increase that should be interpreted as a decrease of the overall mass contained in the total volume of the nanoporous film. The increasingly hydrophobic character found inside the pores and particularly at their walls provokes that the pores of the film may become enriched in molecular catechol, inducing finally the diminution in the QCM frequency experimentally observed.

To further support our explanation, we repeated the same experiment in isobutanol (instead of water) in the presence of 0.1 M $HClO_4$. In this case, the hydrophobic interactions should be minimized. A constant increase in mass is now detected in the whole concentration range (see Fig. 3, ●) together with the typical darkening of the nanoporous layer associated to the formation of the SCTC. The difference between the measured frequency shift and $(\Delta f_\eta + \Delta f_{pore})$ calculated for isobutanol solutions shown in Fig. 3b can be ascribed to catechol adsorption.

The hydrophobic character imparted to TiO_2 surface by the organic substrate to be oxidized (or as a consequence of a deliberate surface modification) may have important consequences in its photocatalytic degradation. Such effects will be particularly important in the case of nanocrystalline films since their pores would tend to have a composition rather different from that found in the solution bulk. The change in the local environment can modify both the efficiency and the selectivity of the photocatalytic process. Photocatalytic reactions not requiring water/hydrophilic species to proceed and being favored by a high concentration of active species (direct hole transfers) would be more efficient and their selectivity increased. This would be the case of oxidative polymerizations initiated by direct electron transfer between the adsorbed compound and the oxide, as is the case of catechol photooxidation under visible light illumination (see below). To take advantage of such a possible improved selectivity, several approaches have been used. For example, it is possible to employ substrates with different hydrophilic/hydrophobic character [47,48] or modify the semiconductor surface with a surfactant [49,50]. The hydrophobic/hydrophilic effects could also occur in suspensions but they are expected to be less important. In the case of films, they should also depend on their porosity. Interestingly, Serpone and co-workers [51] did not found these effects when working with less porous TiO_2 layers. In any case, their presence should be considered as one of the main driving forces explaining the different behavior of suspensions and immobilized nanoparticles.

In the following we evidence and discuss another effect appearing under reactive conditions that can be at the origin of the different behavior of suspensions and sintered films: electron delocalization.

3.3. Raman/fluorescence measurements

As previously mentioned, the adsorption of catechol on TiO_2 and WO_3 leads to the formation of a SCTC. These complexes are able to absorb visible light, inducing interfacial reactivity: it has been demonstrated for TiO_2 that upon light absorption there is an almost instantaneous charge separation [52]. An electron is injected into the semiconductor conduction band leaving behind a positively charged radical at the interface. Most of the electron-hole pairs recombine, but a fraction of them may have long enough lifetimes to react with other species present in solution. As in our Raman spectrometer the excitation line is in

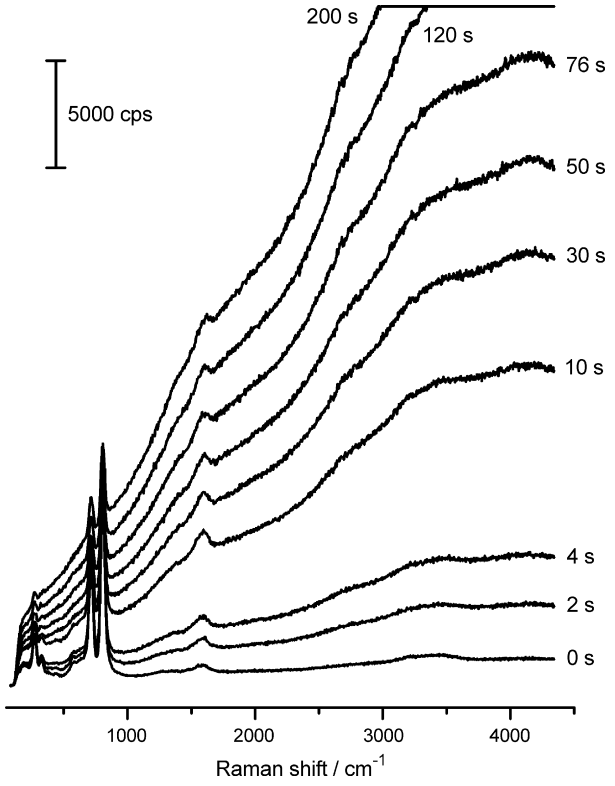

Fig. 4. Raman spectra for a WO_3 nanoporous film on FTO conducting glass in contact with aqueous 14.5 mM catechol and 0.1 M $HClO_4$ solution for different illumination times. The excitation line was provided by an Ar^+ laser at 514.5 nm.

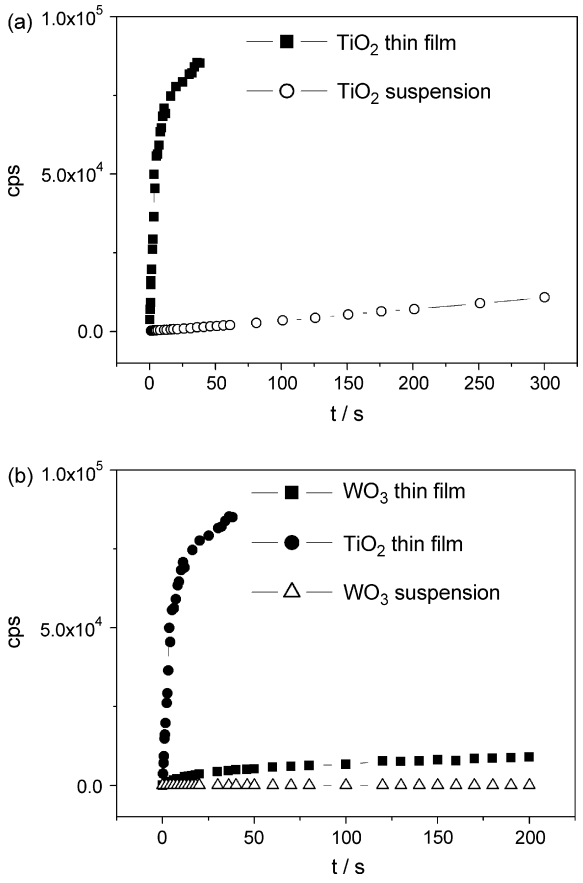

Fig. 5. Time dependence of the fluorescence at 1000 cm^{-1} (a) obtained for an anatase nanostructured film deposited on FTO and for an anatase slurry and (b) obtained for a WO_3 and TiO_2 nanostructured thin films deposited on FTO and for a WO_3 slurry, in contact with a 14.5 mM catechol and 0.1 M $HClO_4$. The excitation line was provided by an Ar^+ laser at 514.5 nm.

the range of the STSC absorption, it can be employed to both induce the reactivity and monitor the possible formation of products. Fig. 4 shows the temporal evolution of the Raman spectra for a WO_3 nanoporous layer. An increasing fluorescence is recorded from the illumination onset, indicating that a reaction occurs and that the product fluoresces. Hence, the rate of fluorescence increase can be associated directly to the product formation rate. Apparently, under illumination the photogenerated cationic radicals react with other catechol molecules located near the surface, giving rise to an oxidative polymerization process, which yields a humic acid-type polymer [19]. Obviously, the reaction rate is limited by the recombination between the photogenerated electrons and adsorbed radicals. An increase in the electron lifetime would induce an increment in the polymerization rate, as the positively charged complex would have more time to react with the surrounding catechol molecules.

Fig. 5(a) shows the time dependence of the fluorescence at $\Delta\bar{\nu} = 1000\,cm^{-1}$ obtained for a sintered anatase film and a slurry. Fig. 5(b) shows the corresponding measurements for akin WO_3 samples. For the sake of comparison, the response of the anatase film has also been included. Two major observations should be highlighted: on the one hand for both oxides the rate of fluorescence is orders of magnitude larger for the thin films than for the concentrated suspensions; on the other hand, such a rate is larger for TiO_2 than for WO_3.

As regards the second observation, one expects the electron photoinjection in the semiconductor to be proportional to the number of catechol molecules adsorbed as catecholate. From the intensity relation of the ATR-IR peaks at 1262 cm^{-1} of Fig. 1, we can estimate that it is about 5.5 times larger for TiO_2. However, the relative difference in the initial slope of both semiconductor films in Fig. 5(b) is considerably larger, i.e. about 50 times. Thus, we can assert that catechol condensation is faster in TiO_2 than in WO_3. This is expected because conduction band electrons are more reductant in the case of TiO_2, favoring its reaction with the oxidant (dissolved oxygen). As photogenerated electrons in WO_3 are not easily consumed in the reduction of oxygen, their recombination is enhanced and consequently the polymerization rate diminishes.

We discuss in the following the first observation: the fluorescence response is highly dependent on the sample nature, increasing faster in the case of thin films. The fluorescence intensity is proportional to the number of fluorophore groups being sampled and can therefore be considered as a relative measure of the amount of polymer formed. Obviously, the amount of oxidized catechol or generated polymer depends on both the reaction rate and the exposed area of the semiconductor in contact with the solution. In our experiment, the film thickness and the slurry concentration were chosen in such a way that the interfacial area sampled by the laser probe was the same in both cases.

Hence, from Fig. 5(a), we can conclude that the photocatalyzed catechol condensation is faster in the case of thin films. If we compare the initial slopes for the slurry and the film, we can estimate that the reaction rate is around 300 times faster for the film. The case WO_3 is even more paradigmatic as no significant fluorescence build-up could be detected for the slurry, whereas the film exhibits an evident and continuous fluorescence growth.

One could link these observations with the results presented in previous sections. First, catechol enrichment due to hydrophobic effects in the pores can partially explain the enhanced photoreactivity of the films. Secondly, in the case of a nanoporous structure with sintered oxide particles, the electron, once injected, can be delocalized throughout the nanoparticle network, thus increasing the distance with the corresponding positively charged radicals. The recombination rate between photogenerated electrons and positively charged residues (holes) would diminish and consequently, the polymerization reaction rate should increase. In the case of particle slurries, the electrons would be restricted to the particle or aggregate of particles, being the average distance between charge carriers much smaller, leading to a higher recombination rate.

In this section we have shown that the behavior of the films can differ from that of the suspensions. Both hydrophobic and electron delocalization effects could underlie these observations. Whereas the existence of the first has been supported by QCM measurements, experimental evidence for the latter is given in the following section on the basis of laterally resolved photoelectrochemical measurements.

3.4. Laterally resolved photoelectrochemical measurements

The electron delocalization can be evidenced using the so-called scanning microscope for semiconductor characterization (SMSC) [21,53], which is a scanning-spot technique. It can provide images of different photoeffects by associating the measured response to the laser location. We have employed a TiO_2 thin film deposited on a conducting glass plate with a groove cut in it of around 0.3 mm in width. As a result, two electrically isolated areas were defined (see sketch in Fig. 6). Briefly, the idea is that if the electrons are able to delocalize inside the porous films, it should be possible to illuminate one of this two areas and detect an increase in the electron concentration in the other (probe electrode). Such a change in free electron concentration is obtained from measurements of the shift in the open circuit potential caused by local illumination. We refer in the following to this shift as photopotential.

Fig. 6 shows the photopotential as a function of the laser-spot position along a line perpendicular to the groove cut in the conducting glass and that crosses it, together with a reflectance profile along the same line. The later allows us to locate the groove as a decrease in reflectance. Only one of the isolated FTO regions separated by the groove (that with $x_0 > 0$) was connected as to measure its open circuit potential (probe electrode). As observed, at $x_0 \leq 0$ the photopotential does not decay sharply to 0, but it slowly diminishes with the distance to

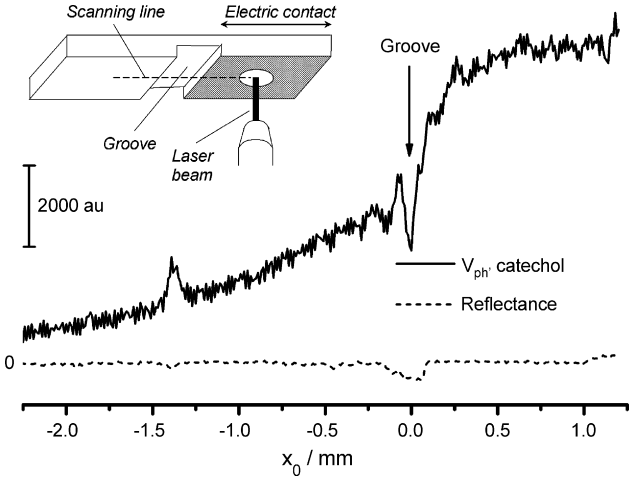

Fig. 6. Photopotential vs. laser spot position in N_2-purged 0.1 M $HClO_4$ and 13.5 mM catechol, together with the reflectance profile showing the location of the groove. Inset: Sketch of the sample.

the probe electrode. Obviously, the photopotential spatial extension depends on the diffusion length (L) of the electrons. In fact, this type of measurement can be employed to determine L [21]. A value as high as 0.4 mm has been found under our experimental conditions. More importantly in the present context, the SMSC experiment shows in a rather direct way that electron delocalization actually occurs in the nanoparticulate layer. Therefore such an effect should also be taken into account when contrasting the behavior of suspensions and immobilized films in photocatalysis. However, it should be noted that under the typical conditions of heterogeneous photocatalysis, which imply the generation of intrinsic electron-hole pairs, the electron diffusion length could be significantly shorter.

4. Conclusions

In this work we have tried to evidence the utility of combining different techniques to study photoinduced reactions using a typical model molecule such as catechol and typical photocatalysts as WO_3 and TiO_2 employed as slurries and thin porous films. We have taken advantage of the complementarity of the different experimental techniques employed, namely ATR-IR and resonance Raman spectroscopies, quartz crystal microbalance and laterally resolved photopotential measurements (SMSC).

ATR-IR and Raman spectroscopies provide vibrational information about the species present at the solution-semiconductor interface. Their high sensitivity (ATR-IR) and high specificity (RRS) furnish a detailed microscopic picture of it. On the other hand, quartz crystal microbalance and photovoltage measurements provide macroscopic information on events happening at the photocatalyst, such as changes in the electron concentration in the porous film or changes in its mass.

Our results show that catechol adsorbs from acidic aqueous solutions on the cationic sites of TiO_2 and WO_3, as a catecholate in a chelating configuration, coexisting in the case of anatase with molecularly adsorbed catechol when its solution concentration is high enough (>1 mM). The chelate is the

species that forms the surface charge complex, as evidenced by resonance Raman spectroscopy, and therefore it is responsible for the visible light photocatalysis. A microscopic detailed understanding of the semiconductor–solution interface is of crucial importance and may prove useful even for the molecular design of photocatalysts. But under working conditions, in addition to the vibrational information obtained at equilibrium (in the dark), information on the adsorption kinetics can also be critical. Interestingly, the adsorption kinetics on nanoporous films can be studied by means of time-resolved ATR-IR measurements. The adsorption of catechol on both oxides can be fitted by the Elovich equation and, significantly, it is initially faster on WO_3 than on TiO_2, which is also a useful piece of information for the design of composite or doped photocatalysts.

Other factors such as mass transport limitations and changes in the hydrophobic–hydrophilic properties might also play an important role in the performance of immobilized photocatalysts. In fact, depending on the catechol solution concentration a significant diminution in mass was detected with the QCM, which can be linked to an increase in pore hydrophobicity imparted by the adsorbed catechol. This type of interaction may provoke important local changes in solution composition inside the nanopores, which may deeply affect both the efficiency and selectivity of the immobilized photocatalyst. Such effects would only be minor in the case of oxide suspensions.

On the other hand, the reactivity under visible light illumination has been studied by Raman spectroscopy, mainly as a way of both photoexciting the sample and measuring the fluorescence associated with the catechol condensation product. Striking differences are found in the rate of the fluorescence development (and thus reaction rate) for suspensions and immobilized thin films, being much larger for the latter. These results constitute a clear example of the different behavior that immobilized and suspended photocatalysts could have even when submitted to equivalent conditions. The hydrophobic effect could be at the origin of the enhanced reactivity of the films, but the possibility of electron delocalization should also be envisaged. In fact, in a sintered nanoparticle network, the electrons photoinjected by the SCTC can delocalize through the film whereas such a delocalization is limited to the aggregate size in the case of suspensions. This delocalization would lead to a lower recombination rate, increasing reactivity. We believe that both hydrophobic–hydrophilic effects and electron delocalization effects should be taken into account when comparing the behavior of immobilized and suspended photocatalysts.

Acknowledgements

Financial support from the Ministerio de Educación y Ciencia (MEC) through projects BQU2003-03737 and CTQ2006-06286/BQU (Fondos FEDER) and from the Generalitat Valenciana through project GV05-119 is greatly acknowledged. D.M.S. is also grateful to the MEC (Spain) for the award of a FPI grant.

References

[1] J.H. Carey, J. Lawrence, H.M. Tosine, Bull. Environ. Contam. Toxicol. 16 (1976) 697.
[2] J.M. Herrmann, Catal. Today 24 (1995) 157.
[3] M.R. Hoffmann, S.J. Martin, W. Choi, D.W. Bahnemann, Chem. Rev. 95 (1995) 69.
[4] A. Mills, S. Le Hunte, J. Photochem. Photobiol. A 108 (1997) 1.
[5] A. Fujishima, T.N. Rao, D.A. Tryk, J. Photochem. Photobiol. C 1 (2000) 1.
[6] O.M. Alfano, D. Bahnemann, A.E. Cassano, R. Dillert, R. Goslich, Catal. Today 58 (2000) 199.
[7] O. Carp, C.L. Huisman, A. Reller, Prog. Solid State Chem. 32 (2004) 33.
[8] K. Kabra, R. Chaudhary, R.L. Sawhney, Ind. Eng. Chem. Res. 43 (2004) 7683.
[9] L.J. Alemany, M.A. Bañares, E. Pardo, F. Martin, M. Galán-Fereres, J.M. Blasco, Appl. Catal. B 13 (1997) 289.
[10] M.F.J. Dijkstra, H. Buwalda, A.W.F. de Jong, A. Michorius, J.G.M. Winkelman, A.A.C.M. Beenackers, Chem. Eng. Sci. 56 (2001) 547.
[11] M.F.J. Dijkstra, A. Michorius, H. Buwalda, H.J. Panneman, J.G.M. Winkelman, A.A.C.M. Beenackers, Catal. Today 66 (2001) 487.
[12] I. Mora-Seró, T. Lana-Villarreal, J. Bisquert, A. Pitarch, R. Gómez, P. Salvador, J. Phys. Chem. B 109 (2005) 3371.
[13] H. Hidaka, H. Honjo, S. Horikoshi, N. Serpone, Catal. Commun. 7 (2006) 331.
[14] M.A. Blesa, A.D. Weisz, P.J. Morando, J.A. Salfity, G.E. Magaz, A.E. Regazzoni, Coord. Chem. Rev. 196 (2000) 31.
[15] T. Lana-Villarreal, J.M. Pérez, R. Gómez, CR Chimie 9 (2006) 806.
[16] A.M. Peiró, J.A. Ayllón, J. Peral, X. Domènech, Appl. Catal. B 30 (2001) 359.
[17] D. Shchukin, S. Poznyak, A. Kulak, P. Pichat, J. Photochem. Photobiol. A 162 (2004) 423.
[18] J. Moser, S. Punchihewa, P.P. Infelta, M. Grätzel, Langmuir 7 (1991) 3012.
[19] T. Lana-Villarreal, A. Rodes, J.M. Pérez, R. Gómez, J. Am. Chem. Soc. 127 (2005) 12601.
[20] D. Monllor-Satoca, L. Borja, A. Rodes, R. Gómez, P. Salvador, Chem. Phys. Chem. 7 (2006) 2540.
[21] T. Lana-Villarreal, D. Monllor-Satoca, R. Gómez, P. Salvador, Electrochem. Commun. 8 (2006) 1784.
[22] P. Araujo, C. Mendive, L. García Rodenas, P. Morando, A.E. Regazzoni, M.A. Blesa, D. Bahnemann, Colloids. Surf. A 265 (2005) 73.
[23] P.C. Redfern, P. Zapol, L.A. Curtiss, T. Rajh, M.C. Thurnauer, J. Phys. Chem. B 107 (2003) 11419.
[24] C. Persson, A. Oskarsson, C. Andersson, Polyhedron 11 (1992) 2039.
[25] Y. Nakayama, H. Saito, A. Nakamura, Chem. Lett. (1996) 691.
[26] P.A. Connor, K.D. Dobson, A.J. McQuillan, Langmuir 11 (1995) 4193.
[27] S.T. Martin, J.M. Kesselman, D.S. Park, N.S. Lewis, M.R. Hoffmann, Environ. Sci. Technol. 30 (1996) 2535.
[28] F. Dumont, P. Verbeiren, C. Buess-Herman, Colloids Surf. A 154 (1999) 149.
[29] R. Rodríguez, M.A. Blesa, A.E. Regazzoni, J. Colloid Interface Sci. 177 (1996) 122.
[30] D.F. Ollis, J. Phys. Chem. B 109 (2005) 2439.
[31] A. Mills, J. Wang, D.F. Ollis, J. Phys. Chem. B 110 (2006) 14386.
[32] P.A. Connor, A.J. McQuillan, Langmuir 15 (1999) 2916.
[33] D.M. Smith, W.F. Welch, J.A. Jassim, A.R. Chughtai, D.H. Stedman, Appl. Spectrosc. 42 (1988) 1473.
[34] R.-S. Juang, M.-L. Chen, Ind. Eng. Chem. Res. 36 (1997) 813.
[35] Z. Hongshao, R. Stanforth, Environ. Sci. Technol. 35 (2001) 4753.
[36] J. Zhang, R. Stanforth, Langmuir 21 (2005) 2895.
[37] B. Gao, Y. Ma, Y. Cao, W. Yang, J. Yao, J. Phys. Chem. B 110 (2006) 14391.
[38] B.I. Lemon, J.T. Hupp, J. Phys. Chem. 100 (1996) 14578.
[39] S. Si, K. Huang, X. Wang, M. Huang, H. Chen, Thin Solid Films 422 (2002) 205.
[40] R. Morand, K. Noworyta, J. Augustynski, Chem. Phys. Lett. 364 (2002) 244.
[41] T. Lana-Villarreal, R. Gómez, in preparation.

[42] K.K. Kanazawa, J.G. Gordon, Anal. Chem. 57 (1985) 1770.
[43] P. Schön, R. Michalek, L. Walder, Anal. Chem. 71 (1999) 3305.
[44] L.E. Swearingen, J. Phys. Chem. 32 (1928) 785.
[45] D.A. Buttry, M.D. Ward, Chem. Rev. 92 (1992) 1355.
[46] L. Daikhin, E. Gileadi, V. Tsionsky, M. Urbakh, G. Zilberman, Electrochim. Acta 45 (2000) 3615.
[47] K. Shimizu, H. Murayama, A. Nagai, A. Shimada, T. Hatamachi, T. Kodama, Y. Kitayama, Appl. Catal. B 55 (2005) 141.
[48] C. Ooka, H. Yoshida, K. Suzuki, T. Hattori, Appl. Catal. A 260 (2004) 47.
[49] H. Tada, H. Matsui, F. Shiota, M. Nomura, S. Ito, M. Yoshihara, K. Esumi, Chem. Commun. (2002) 1678.
[50] K. Inumaru, M. Murashima, T. Kasahara, S. Yamanaka, Appl. Catal. 52 (2004) 275.
[51] H. Hidaka, H. Honjo, S. Horikoshi, N. Serpone, New J. Chem. 27 (2003) 1371.
[52] T. Rajh, L.X. Chen, K. Lukas, T. Liu, M.C. Thurnauer, D.M. Tiede, J. Phys. Chem. B 106 (2002) 10543.
[53] A.M. Chaparro, P. Salvador, B. Coll, M. González, Surf. Sci. 293 (1993) 160.